UC Irvine
UC Irvine Previously Published Works

Title

Influence of optical properties on two-photon fluorescence imaging in turbid samples.

Permalink
https://escholarship.org/uc/item/8x22h9rb

Journal
Applied optics, 39(7)

ISSN
1559-128X

Authors

Dunn, AK
Wallace, VP
Coleno, M
et al.

Publication Date
2000-03-01

DOI
10.1364/ao.39.001194

Copyright Information
This work is made available under the terms of a Creative Commons Attribution License, availalbe at https://creativecommons.org/licenses/by/4.0/

Peer reviewed

eScholarship.org Powered by the California Digital Library
University of California

Influence of optical properties on two-photon fluorescence imaging in turbid samples

Andrew K. Dunn, Vincent P. Wallace, Mariah Coleno, Michael W. Berns,
and Bruce J. Tromberg

A numerical model was developed to simulate the effects of tissue optical properties, objective numerical aperture (N.A.), and instrument performance on two-photon-excited fluorescence imaging of turbid samples. Model data are compared with measurements of fluorescent microspheres in a tissuelike scattering phantom. Our results show that the measured two-photon-excited signal decays exponentially with increasing focal depth. The overall decay constant is a function of absorption and scattering parameters at both excitation and emission wavelengths. The generation of two-photon fluorescence is shown to be independent of the scattering anisotropy, g, except for $g > 0.95$. The N.A. for which the maximum signal is collected varies with depth, although this effect is not seen until the focal plane is greater than two scattering mean free paths into the sample. Overall, measurements and model results indicate that resolution in two-photon microscopy is dependent solely on the ability to deliver sufficient ballistic photon density to the focal volume. As a result we show that lateral resolution in two-photon microscopy is largely unaffected by tissue optical properties in the range typically encountered in soft tissues, although the maximum imaging depth is strongly dependent on absorption and scattering coefficients, scattering anisotropy, and objective N.A.. © 2000 Optical Society of America

OCIS codes: 180.0180, 170.3660, 170.0180.

1. Introduction

Two-photon fluorescence microscopy has shown great promise as a means of obtaining high-resolution, three-dimensional images of tissue at depths that can exceed those obtained with confocal fluorescence techniques. In two-photon fluorescence imaging, near-infrared light is used to excite transitions of twice the energy of a single photon. Since the absorption probability is proportional to the square of the instantaneous intensity of the excitation light, the generated fluorescence is confined to a small region around the focal volume, making the technique inherently depth resolved. For high-numerical-aperture (N.A.) microscope objectives this volume is of the order of a femtoliter.

Depth-resolved imaging of tissue by use of two-photon fluorescence was first demonstrated by Denk *et al.*[1] One of the advantages of two-photon fluorescence over conventional fluorescence imaging is that near-infrared light is used, which penetrates more deeply into tissue, owing to decreased scattering. Recent applications of intravital, two-photon fluorescence imaging have included video-rate imaging of skin[2] and imaging of blood flow in exposed rat neocortex.[3] In general the investigators in Refs. 1–3 were able to image structure and function at depths between 300 and 600 μm.

Other techniques such as confocal microscopes and optical coherence tomography provide the ability to obtain depth-resolved images, but each has limitations on resolution and imaging depth. Although it is understood that scattering is the primary factor that limits the imaging depth of these techniques, the detailed factors that influence this depth are not completely understood. Scattering plays a role in limiting the imaging depth by decreasing the number of excitation photons reaching the focus area and by decreasing the number of fluorescent photons collected by the objective lens. These effects can be studied by examination of how both temporal and spatial components of the source point-spread function (PSF) are affected by scattering.

In this paper the detailed influence of tissue optical

When this research was performed, the authors were with the Laser Medical and Microbeam Program, Beckman Laser Institute, University of California, Irvine, California 92612. A. K. Dunn is now with the NMR Center, Massachusetts General Hospital, Harvard Medical School, Charlestown, Massachusetts 02129. B. J. Tromberg's e-mail address is tromberg@bli.uci.edu.

Received 3 August 1999; revised manuscript received 7 December 1999.

0003-6935/00/071194-08$15.00/0

© 2000 Optical Society of America

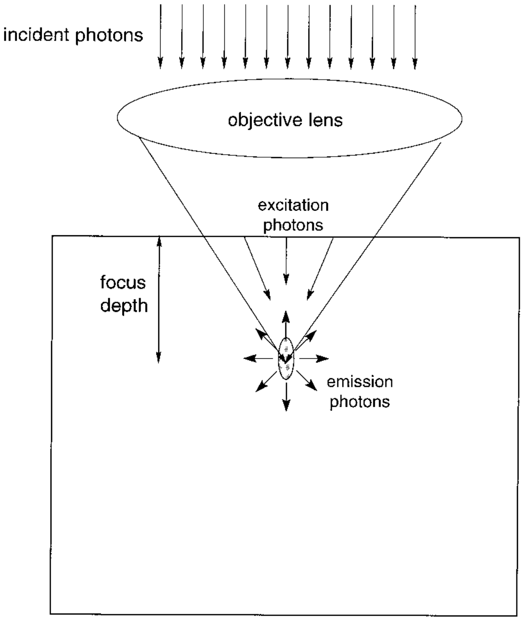

Fig. 1. Geometry used in the Monte Carlo simulation.

properties and instrument parameters on the two-photon fluorescence signal is described with a Monte Carlo model. Because of their flexibility, Monte Carlo models have been used to characterize different imaging modalities in highly scattering media.[4–8] Two-photon fluorescence images of fluorescent spheres embedded in turbid gels are used to validate the model and assess instrument performance. Our results show that two-photon microscopy can be used to form high-resolution images at depths as great as 400 μm in typical nonkeratinized epithelial tissues. The overall signal intensity is a function of instrument parameters including source pulse width, objective N.A., tissue optical properties, and the photophysical characteristics of the fluorophore. Although the two-photon fluorescence signal intensity decreases as a result of scattering-induced losses in the ballistic photons, image resolution is essentially unaffected by tissue optical properties. As a result transform-limited resolution can be obtained at depths of 2–5 times the scattering mean free path.

2. Theory and Model

The Monte Carlo model was split into two halves: excitation of two-photon fluorescence and collection of the emitted fluorescent photons. In the calculation of the two-photon excitation, photons were launched into the tissue in a focused beam geometry as illustrated in Fig. 1. Photons were uniformly distributed at the objective lens, and the initial direction of each photon was determined from the focal depth and the starting point on the objective lens. The initial directions were varied so that, in the absence of tissue scattering, the intensity profile at the focus would approximate a diffraction-limited spot. Aberrations caused by the objective lens were not taken into account in the model, since our focus in this study is to quantify the dominant effects of multiple light scattering in the tissue.

As each photon propagated through the medium, the coordinates $\mathbf{r} = (x, y, z)$ of all interaction points were recorded and stored for postprocessing. Each photon was propagated until it was either absorbed; reflected out of the medium; or had a path length that exceeded a preset value, which was usually ten times the focal depth. This value was varied to ensure that it did not alter the results. Although the model included single-photon absorption through the absorption coefficient, μ_a, it was assumed that multiphoton absorption did not alter the distribution of excitation light within the medium.

Once the simulation was run and the entire photon trajectories for all photons stored, the spatial and temporal distribution of photons, $G(\mathbf{r}, t)$, that was due to an infinitely short pulse was known. To determine the spatial and temporal distribution of photons due to a laser pulse of specified pulse width and energy, the temporal impulse response at each spatial point within the medium was convolved with the laser pulse profile

$$I_{\mathrm{ex}}(\mathbf{r}, t) = \int_{-\infty}^{\infty} G(\mathbf{r}, t')f(t - t')\mathrm{d}t', \tag{1}$$

where $G(\mathbf{r}, t)$ is the impulse response and $f(t)$ is the temporal laser pulse profile. A Gaussian temporal profile was assumed throughout this study. In Eq. (1), $I_{\mathrm{ex}}(\mathbf{r}, t)$ represents the spatial and temporal distribution of the excitation light in the medium.

The spatial distribution of generated two-photon fluorescence sources within the medium, $F_{\mathrm{ex}}(\mathbf{r})$, is related to the square of the instantaneous intensity of the excitation light,

$$F_{\mathrm{ex}}(\mathbf{r}) = \frac{1}{2}\,\phi\sigma C(\mathbf{r}) \int_{-\infty}^{\infty} I_{\mathrm{ex}}{}^2(\mathbf{r}, t)\mathrm{d}t, \tag{2}$$

where ϕ is the fluorescence quantum efficiency, σ is the two-photon absorption cross section, and $C(\mathbf{r})$ is the spatially dependent fluorophore concentration.[9]

To determine the fraction of the generated two-photon fluorescence collected by the detector, the second half of the Monte Carlo simulation was used. Fluorescent photons were launched from within the sample with a spatial distribution given by $F_{\mathrm{ex}}(\mathbf{r})$ and with isotropic initial directions. The optical properties of the sample were those at the emission wavelength. The fluorescent photons were propagated until they were either absorbed or exited the medium. For those photons exiting the top surface of the sample a geometrical ray trace was performed to determine whether the photon was collected by the objective lens. This procedure was similar to that used in confocal Monte Carlo models,[4,6] although a pinhole was not used at the detector.

Once the fraction of fluorescent photons reaching the detector, $F_{\mathrm{em}}(\mathbf{r})$, was determined with the second half of the simulation, the total number of photons reaching the detector due to a single laser pulse fo-

Table 1. Optical Properties of the 2% Intralipid Agarose Gel Used in the Measurements and Simulations at the Excitation and Emission Wavelengths[a]

Wavelength (nm)	μ_s (mm^{-1})	μ_a (mm^{-1})	g
780	6	4×10^{-4}	0.65
515	16	4×10^{-4}	0.8

[a] Values taken from van Staveren *et al.* (Ref. 14).

cused at a depth, z_f, could be determined from the product of the generation and collection of fluorescence,

$$S(z_f) = \eta \int F_{\mathrm{ex}}(\mathbf{r}) F_{\mathrm{em}}(\mathbf{r}) \mathrm{d}\mathbf{r}, \tag{3}$$

where $F_{\mathrm{em}}(\mathbf{r})$ describes the fraction of fluorescent photons generated at $\mathbf{r}$ that reach the surface within the acceptance angle of the objective lens and η describes the collection efficiency of the optics, filters, and detector quantum efficiency.

With the two-part simulation the dependence of the optical properties of the medium on the generation and collection of two-photon fluorescence at increasing focal depths was studied for each set of optical properties. The resulting detector signal as a function of focal depth, $S(z_f)$, was fitted to a function of the form

$$S(z_f) = S_o \exp[-(b_{\mathrm{ex}}\mu_t^{\mathrm{ex}} + b_{\mathrm{em}}\mu_t^{\mathrm{em}}) z_f], \tag{4}$$

where μ_t^{ex} and μ_t^{em} are the total attenuation coefficients ($\mu_t = \mu_s + \mu_a$) at the excitation and emission wavelengths, respectively, and b_{ex} and b_{em} are parameters determined by means of fitting the computed decay of the generation and collection of two-photon fluorescence. The term S_{o} in Eq. (2) is the amount of fluorescence generated in a nonscattering medium for the same N.A., fluorophore concentration, and quantum efficiency. The fluorophore concentration, $C(\mathbf{r})$, was assumed to be uniform over the entire sample in all simulations.

3. Experiment

The simulated results were compared with measurements of the depth-dependent signal decay of a point emission source in a scattering sample. The sample consisted of 0.1-μm-diameter fluorescent spheres (Fluorospheres, F-8803, Molecular Probes) suspended in an agarose gel matrix. Intralipid (20% solids, Baxter) was added to the gelatin at a final concentration of 2% to provide background scattering comparable with that found in tissues. The scattering and absorption coefficients at the excitation (780 nm) and emission (515 nm) wavelengths are listed in Table 1. The optical properties of the gel were verified by measurement of the reduced scattering coefficient, $\mu_s' = \mu_s(1 - g)$, and the absorption coefficient, μ_a, with a frequency domain photon migration instrument described in Ref. 10. The gelatin–sphere mixture was placed on a glass slide before being solidified and covered with a coverslip.

The two-photon microscope system used in the measurements consists of a mode-locked titanium sapphire laser with a pulse width of approximately 100 fs and a repetition rate of 76 MHz (Coherent, Mira Model 900) and an inverted microscope (Zeiss, Axiovert Model 135). The beam is scanned across the sample with orthogonal galvanometric mirrors (Cambridge Technology) and focused onto the sample with a 63×, 1.2-N.A. microscope objective (Zeiss c-Apochromat). The two-photon fluorescence is split off from the excitation light with a dichroic beam splitter, and excess excitation light is suppressed by placement of bandpass filters in front of the detector. The fluorescent light is detected with a single-photon counting detection system consisting of a photomultiplier tube (Hamamatsu Model R5600P) and a 100-MHz single-photon counting amplifier–discriminator (Advanced Research Instruments, Model F-100T). Typically images (256 × 256 pixels) are acquired at a rate of 1 frame/s with an excitation power of ~10 mW at the sample. Beam scanning and image acquisition are computer controlled through a data acquisition board developed at the Laboratory for Fluorescence Dynamics at the University of Illinois, Urbana-Champaign.

To analyze the decay of the two-photon fluorescence signal with depth, images were acquired at depth intervals of 20 μm from the surface of the sample to a maximum depth of 250 μm, which corresponded to the working distance of the objective. Within each image the signal intensity was quantified by calculation of the average intensity of approximately 25 individual spheres. The width of the lateral PSF was approximated by means of fitting the lateral intensity profile of each sphere to a Gaussian function.

4. Results

A. Simulation

Simulations were run to investigate the effects of scattering on the generation and collection of fluorescent light. Figure 2 illustrates the effect of the scattering coefficient on the generation and collection of two-photon fluorescence as a function of focus depth in the sample. In these simulations the scattering coefficients of the medium were varied at 5, 10, and 15 mm, and the anisotropy and absorption coefficients were held fixed at $g = 0.9$ and $\mu_a = 0.01\ \mathrm{mm}^{-1}$, respectively. The objective N.A. was 1.3, and the pulse width and repetition rate were 100 fs and 76 MHz, respectively. The excitation data at each set of optical properties were fit to an exponential decay of the form $\exp(-b_{\mathrm{ex}}\mu_t^{\mathrm{ex}} z)$, where μ_t^{ex} is the total attenuation coefficient at the excitation wavelength and z is the focal depth. The parameter b_{ex} was used as a measure of the rate of decay of the excitation with depth. For the excitation data shown in Fig. 2 the fit coefficients, b_{ex}, were 2.63, 2.69, and 2.53 for scattering coefficients of 5, 10, and 15 mm, respectively.

The collection efficiency was computed for the same

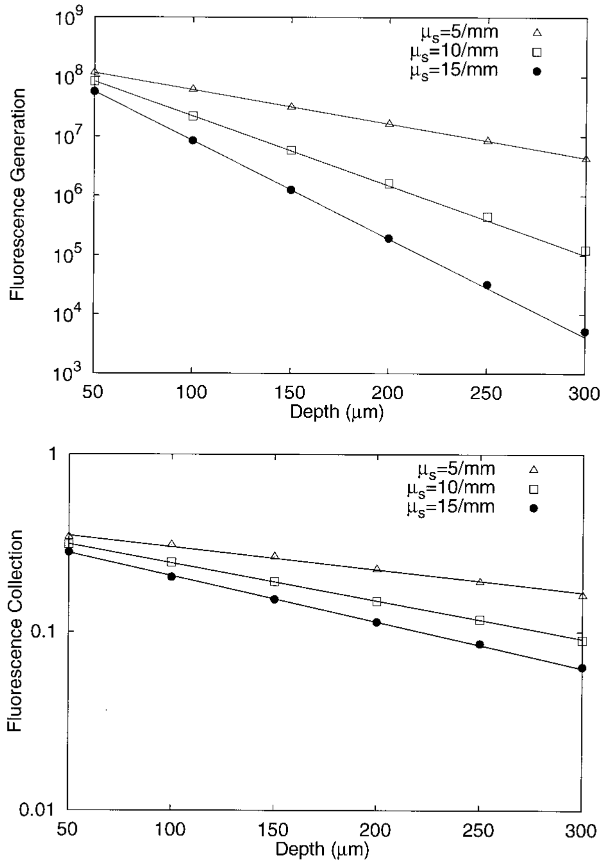

Fig. 2. Fluorescence generation (top) and collection (bottom) at three different scattering coefficients (5, 10, and 15 mm^{-1}). Solid curves, exponential fits to the data.

three scattering coefficients, and the results are shown in Fig. 2 as a function of depth. These data were also fit to an exponential decay of the form $\exp(-b_{\text{em}}\mu_t^{\text{em}}z)$, and the fit coefficients, b_{em}, were 0.59, 0.49, and 0.40 for scattering coefficients of 5, 10, and 15 mm, respectively. Comparison of the generation and collection efficiency decay rates shows that the generation of two-photon fluorescence falls off with depth considerably faster than does the signal collection.

The effect of the scattering anisotropy, g, on the generation of two-photon fluorescence is shown in Fig. 3. The generated fluorescence intensity is plotted as a function of anisotropy for a focal depth of 200 μm, a N.A. of 1.3, and a pulse width of 100 fs. The fluorescence intensity remains relatively constant for all values of $g < 0.95$, after which it rises sharply.

In addition to the optical properties of the sample, the N.A. can play an important role in determining the amount of two-photon fluorescence generated and collected. Typically a high-N.A. (1.0–1.4) objective is used to obtain the smallest possible spot size and therefore to generate the largest amount of fluorescence. To study the role that the N.A. plays in two-photon imaging in highly scattering samples, simulations were run at focal depths of 100, 200, and 300 μm for N.A.'s ranging between 0.2 and 1.3. The

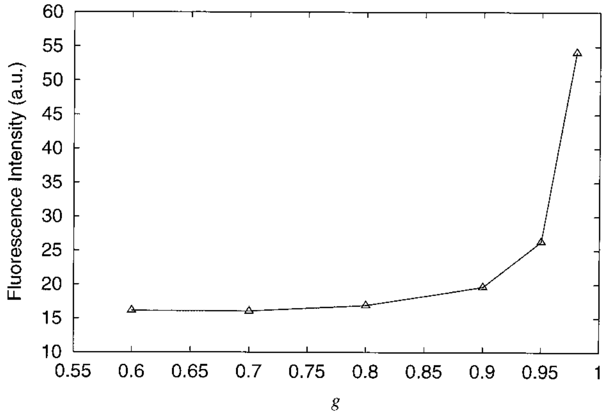

Fig. 3. Effect of anisotropy, g, on the generation of two-photon fluorescence at a focus depth of 200 μm.

optical properties of the sample were $\mu_s = 10$ mm, $\mu_a = 0.005$ mm, and $g = 0.9$. In the simulations N.A.'s between 0.6 and 1.0 were water-immersion objectives, and those greater than 1.0 were oil-immersion objectives.

The total detected two-photon fluorescence is plotted in Fig. 4 as a function of N.A. We computed the detected fluorescence by taking the product of the generated fluorescence and the collection efficiency from the two parts of the simulation. At a focus depth of 100 μm the detected fluorescence increases as the N.A. increases. However, at depths of 200 and 300 μm the detected fluorescence peaks at a N.A. of ~0.6, suggesting that the optimal two-photon microscopy N.A. varies with depth.

B. Experiment

An example image 100 μm into the tissue phantom is shown in Fig. 5. Individual 0.1-μm fluorescent spheres are visible in the image, and a single sphere is shown in Fig. 5(b). A Gaussian fit to the pixel intensities is shown in Fig. 5(c) illustrating the procedure that was followed to measure the signal characteristics as a function of depth. The intensity at a given focal depth was determined from the average

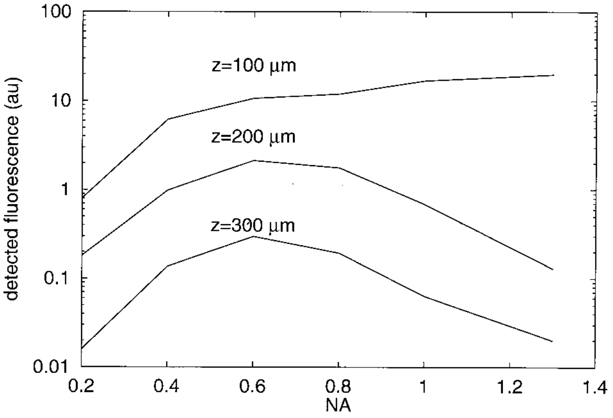

Fig. 4. Total detected fluorescence intensity as a function of objective N.A. for focal depths of 100, 200, and 300 μm.

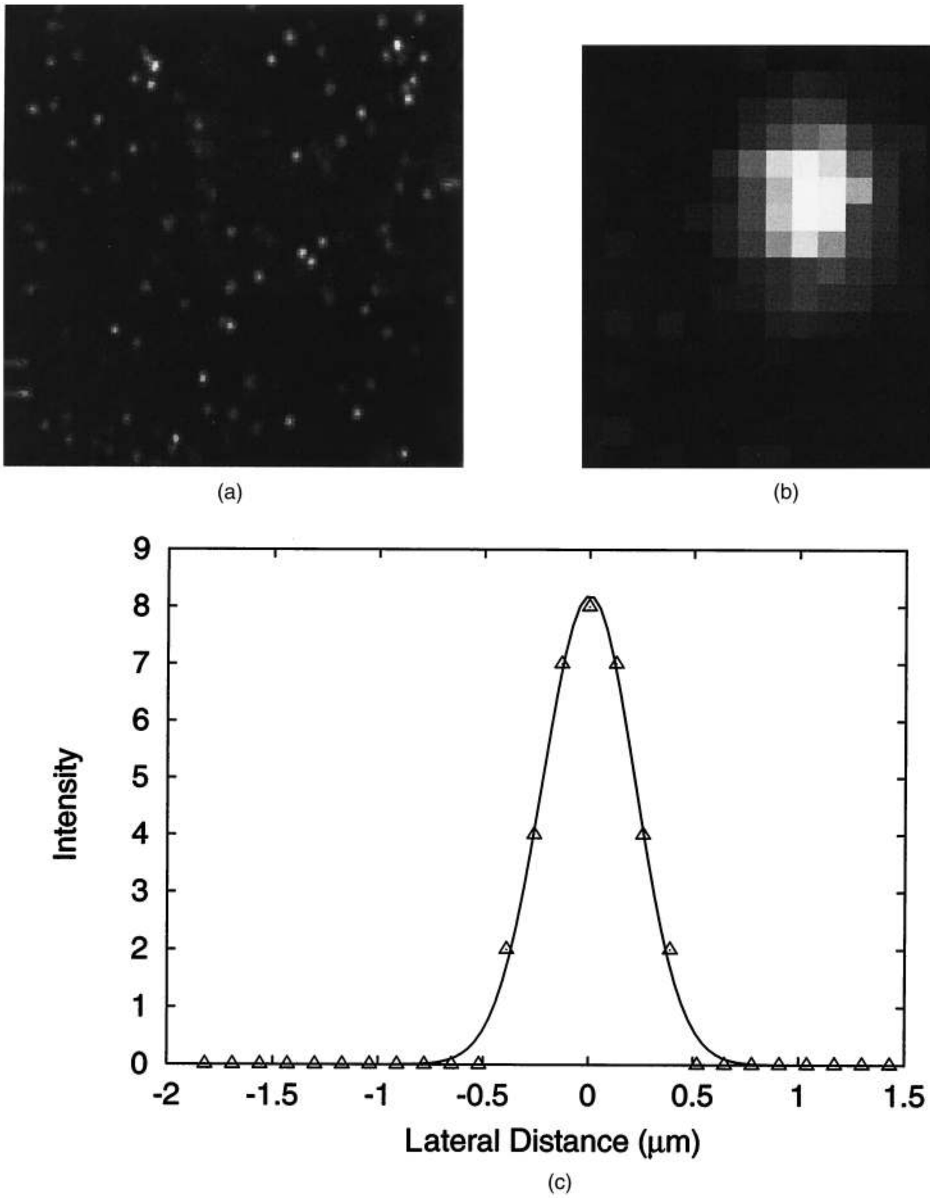

Fig. 5. Measurement of the lateral PSF of the system. (a) Image of the tissue phantom at a depth of approximately 100 μm. (b) Image of an individual sphere from the image in (a). (c) Gaussian fit to the intensity of a single sphere.

amplitude of the Gaussian fits to approximately 25 spheres. The width of the lateral PSF was estimated from the $1/e$ decay of the Gaussian profile.

The results of the phantom measurements are plotted in Figs. 6 and 7. The depth-dependent intensity decay was fitted to an exponential of the form $\exp(-az)$. This form is slightly different from that used for the simulated data, since the generation and collection processes cannot be separated in the experiment. Therefore the fit parameter, a, in the measured data is related to the simulated data by $a = b_{\mathrm{ex}}\mu_t^{\mathrm{ex}} + b_{\mathrm{em}}\mu_t^{\mathrm{em}}$. The value of a determined from the fit shown in Fig. 6 was 16 cm^{-1}.

The measured width of the spheres shows no significant change to a depth of 250 μm, roughly the working distance of the objective. The theoretical width of the lateral PSF in a nonscattering medium

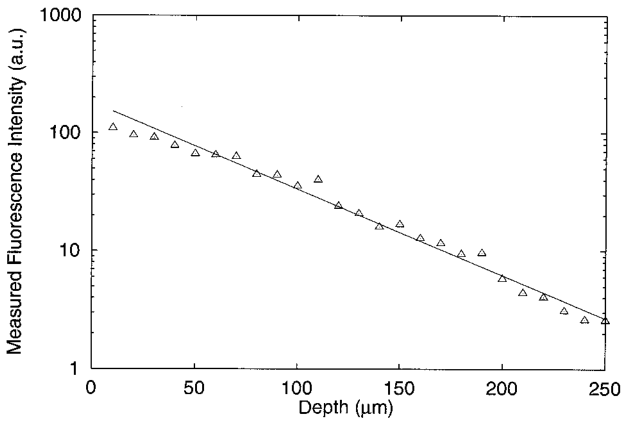

Fig. 6. Measured two-photon fluorescence as a function of focal depth for 0.1-μm fluorescent spheres embedded in a 2% intralipid phantom ($\mu_s^{\mathrm{ex}} = 6\ \mathrm{mm}^{-1}$, $\mu_s^{\mathrm{em}} = 16\ \mathrm{mm}^{-1}$).

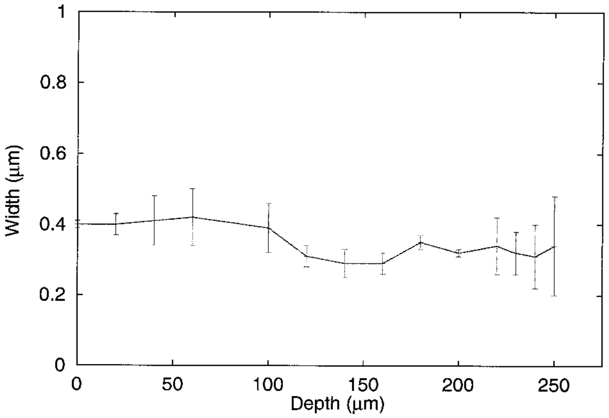

Fig. 7. Measured width of 0.1-μm fluorescent spheres embedded in 2% intralipid as a function of focal depth. The width at each depth is the average width of approximately 25 spheres as measured by Gaussian fits to the individual spheres.

for this set of parameters is approximately 0.35 μm,[11] which is close to the measured value.

5. Discussion

The signal degradation was decomposed into two components in our model: attenuation of excitation photons and attenuation of fluorescence. The product of the two components yields a quantity proportional to the measured signal intensity. Figure 2 illustrates the two components at different levels of scattering and shows that each is well described by an exponential attenuation. The slope of the exponential decay for the collection efficiency of the fluorescent photons ranges between 0.4 and 0.59. Since this value is less than unity (i.e., $b_{\mathrm{em}} = 1$ for single-scattering behavior), there is a clear indication that multiply scattered photons are collected by the objective lens and subsequently detected. The excitation of two-photon fluorescence however, decays more rapidly with a relatively large decay coefficient, b_{ex}, of ~2.5. Since $b_{\mathrm{em}} = 2$ would be expected for single-scattering attenuation in a two-photon process, this suggests that ballistic photons are the primary source of excitation. The calculated value of 2.5 suggests that the average photon path length is slightly greater than the linear distance between the sample surface and the focal plane. This observation is consistent with our understanding of the enhanced scattering probability for high-incidence-angle photons emerging from high-N.A. objectives.

In two-photon imaging, objectives with the highest available N.A. are typically used, since this results in the smallest spot size and the greatest instantaneous excitation intensity. In highly scattering media a trade-off exists between the smallest spot size and the increased attenuation of excitation photons at high N.A.'s. This is because photons propagating along the outer cone of light at high-objective N.A.'s have an incidence angle as high as 60°. Although this effect is not seen in transparent media, in turbid samples these photons must travel a longer distance to reach the focus. Because of the higher probability of long-path-length photons undergoing scattering events, fewer photons may be available for excitation.

As illustrated in Fig. 4, the impact of N.A. on the detected fluorescence changes with depth. At a depth of 100 μm (1 mean free path), increasing the N.A. improves signal collection. In contrast, at depths of 200 and 300 μm the optimal N.A. is between 0.6 and 0.8. Although the high N.A.'s still produce a smaller spot size than do the lower N.A.'s at these depths, the increased probability of scattering for high-angle paths leads to their selective attenuation and a decrease in the overall detected signal.

A similar effect has been observed in reflectance imaging of turbid samples[5] although the mechanism differs. In reflectance imaging a low N.A. can result in higher resolution, since fewer multiply scattered photons are collected, whereas in two-photon imaging a lower N.A. is advantageous, since it results in an increase in the number of fluorescent photons generated. As shown in Fig. 2, multiply scattered emission light is collected, and therefore a higher N.A. is beneficial at all depths for optimal collection of fluorescent light. This suggests that the optimal combination would be to use a lower N.A. for excitation and a high N.A. to collect the emission, which could be accomplished by means of underfilling the microscope objective in the back focal plane.

Figure 3 demonstrates that the anisotropy factor, g, can significantly alter the generation of two-photon fluorescence at values above ~0.95. At lower values of g (<0.95) the generation of fluorescence is dominated by photons reaching the focus unscattered. Those photons that are scattered encounter an angular deviation sufficiently large to prevent them from reaching the focus and therefore contribute very little to the generation of fluorescence. At higher values of g, however, the angular deviation imparted to a photon upon scattering is sufficiently small to permit the photon to reach the focal volume and contribute to the excitation. Although values of g for tissue are typically ~0.9 (Ref. 12), g is significantly higher for cells with values between 0.95 and 0.99 (Ref. 13). Therefore, when imaging tissues such as densely packed epithelial cell layers, photons may encounter multiple small-angle scattering and still contribute to the generation of two-photon fluorescence.

The measured signal decay in the tissue phantom (Fig. 6) demonstrates that the detected fluorescence signal declines exponentially with depth as predicted by the model. By fitting Eq. (4) to the measured data, a total decay constant is calculated to be 16 mm^{-1}. This value is comparable with model simulations for 2% intralipid, which range between 19 and 26 mm^{-1} assuming a 10% uncertainty in the optical properties of the intralipid. This measured decay coefficient, a, is actually a composite function of the optical properties at the excitation and emission wavelengths ($a = b_{\mathrm{ex}}\mu_t^{\mathrm{ex}} + b_{\mathrm{em}}\mu_t^{\mathrm{em}}$), and our calculated values show excellent agreement with previ-

Table 2. Optical Properties of Cervical Epithelium Used in the Estimation of Imaging Depth[a]

Wavelength (nm)	μ_s (mm^{-1})	μ_a (mm^{-1})	g
811	5.5	0.002	0.9
674	90	0.003	0.9

[a] The absorption and reduced scattering coefficients were taken from Ref. 18, and g was assumed to be 0.9.

ously reported measurements of the optical properties of 2% intralipid.[14]

The lateral resolution is unaffected by scattering up to a depth of 250 μm as illustrated in Fig. 7, where the measured width of the lateral point spread remains relatively constant. This indicates that the limiting factor in imaging in turbid samples is a lack of signal rather than a loss of resolution, which is in agreement with previous studies of confocal[15] and two-photon[16] imaging.

With the expression for the two-photon fluorescence signal decay given by Eq. (4), predictions on the maximum imaging depth can be made for a given set of experimental parameters and tissue optical properties on the basis of an estimation of the signal-to-noise ratio. The signal-to-noise ratio in photon-counting mode can be written as[17]

$$\mathrm{SNR} = \frac{N_s \sqrt{t}}{[N_s + 2(N_d + N_b)]^{1/2}}, \tag{5}$$

where N_s is the number of fluorescence photons/s that can be computed from Eq. (5), N_b and N_d are the number of background and dark counts/s, and t is the integration time. To predict the maximum imaging depth for two-photon imaging in nonkeratinized squamous epithelial tissue with an exogenous fluorophore, the *in vivo* measured optical properties of cervix[18] at the excitation and emission wavelengths, listed in Table 2, were used.

Chloroaluminum sulfonated phthalocyanine (CASPc) is a widely used photodynamic therapy (PDT) agent[19] and an efficient two-photon fluorophore. The concentration of CASPc was assumed to be 50 μM, and the two-photon absorption cross section of CASPc was estimated by comparison of the two-photon fluorescence emission properties of CASPc with that of a known compound,[20] Rhodamine B, whose two-photon cross section has been measured.[9] By numerical integration of the measured two-photon fluorescence emission spectra of CASPc and Rhodamine B (data not shown), the two-photon cross section of CASPc was estimated to be $1.7 \times 10^{-49}\ \text{cm}^4$ s/photon.

The objective N.A. was assumed to be 1.3, and the laser characteristics were those of a typical mode-locked titanium sapphire source (76-MHz repetition rate and 100-fs pulse width) with an average power of 10 mW at the sample. The detector was assumed to have a quantum efficiency of 0.2 with a dark count, $N_d = 20$ counts/s, and a background level of 100 counts/s.[17] The image is 256 × 256 pixels with an acquisition time of 2 s.

On the basis of these values and with Eqs. (4) and (5), the signal level and the signal-to-noise ratio can be estimated for a complete set of experimental parameters and tissue characteristics. The term S_o in Eq. (4) represents the signal intensity in the absence of scatter and can be calculated as described in Ref. 9.

The maximum imaging depth can then be determined through a calculation of the depth at which the signal-to-noise ratio falls below a given value. Assuming a minimum signal-to-noise ratio of 3, the maximum imaging depth for cervical epithelial tissue with CASPc as the fluorophore with the experimental parameters outlined above is predicted to be 412 μm. Therefore, with this procedure, the predicted imaging depth and signal-to-noise ratio can be studied for a complete set of experimental conditions including laser source characteristics, tissue optical properties, and fluorophore properties.

6. Conclusions

With a Monte Carlo model and measurements on tissue phantoms, the characteristics of the two-photon fluorescence signal with depth in a highly scattering medium have been investigated. The model and measurements have shown that the two-photon excited fluorescence signal in a highly scattering medium is dependent on the properties of the medium and the instrument. Fluorescence was found to decay exponentially with a slope determined by the scattering and absorption coefficients of the medium at the excitation and emission wavelengths. The scattering anisotropy influences the generation of two-photon fluorescence only at values greater than 0.95, where multiply scattered photons can still contribute to the signal. The optimal objective N.A. was found to vary with focal depth, illustrating the trade-off between a higher instantaneous excitation intensity at high N.A.'s and the increased probability of scattering for photons entering turbid samples at high incidence angles. The model predictions for the decay of the two-photon signal with depth were comparable with the measured decay in a turbid phantom. On the basis of the predicted form of the two-photon signal decay with depth and a minimum acceptable signal-to-noise ratio, the maximum imaging depth can be predicted for a complete set of experimental parameters. For the case of two-photon imaging of cervical epithelial tissue, the maximum imaging depth is predicted to be approximately 412 μm assuming a fluorophore with characteristics similar to chloroaluminum sulfonated phthalocyanine (CASPc).

This study was supported by National Institutes of Health grants RR-01192 and GM-50958; the Office of Naval Research (ONR #N00014-91-C-0134), and the Department of Energy (DOE #DE-FG03-91ER61227). Assistance from Peter So, Enrico Gratton, and the Laboratory for Fluorescence Dynamics in the construction of the two-photon microscope is gratefully acknowledged.

References

1. W. Denk, J. Strickler, and W. Webb, "Two-photon laser scanning fluorescence microscopy," Science **248,** 78–76 (1990).
2. K. H. Kim, C. Buehler, C.-Y. Dong, B. R. Masters, and P. T. C. So, "Tissue imaging using two-photon video rate microscopy," in *Optical Diagnostics of Living Cells II*, D. L. Farkas, R. C. Leif, and B. J. Tromberg, Proc. SPIE **3604,** 60–66 (1999).
3. D. Kleinfeld, P. Mitra, F. Helmchen, and W. Denk, "Fluctuations and stimulus-induced changes in blood flow observed in individual capillaries in layers 2 through 4 of rat neocortex," Proc. Natl. Acad. Sci. USA **95,** 15741–15746 (1998).
4. J. Schmitt, A. Knuttel, and M. Yadlowski, "Confocal microscopy in turbid media," J. Opt. Soc. Am. A **11,** 2226–2235 (1994).
5. X. Gan, S. Schilders, and M. Gu, "Image formation in turbid media under a microscope," J. Opt. Soc. Am. A **15,** 2052–2058 (1998).
6. A. Dunn, C. Smithpeter, R. Richards-Kortum, and A. J. Welch, "Sources of contrast in confocal reflectance imaging," Appl. Opt. **35,** 3441–3446 (1996).
7. D. Smithies, T. Lindmo, Z. Chen, J. Nelson, and T. Milner, "Signal attenuation and localization in optical coherence tomography studied by Monte Carlo simulation," Phys. Med. Biol. **43,** 3025–3044 (1998).
8. X. Gan and M. Gu, "Effective point-spread function for fast image modeling and processing in microscopic imaging through turbid media," Opt. Lett. **24,** 741–743 (1999).
9. C. Xu and W. Webb, "Measurement of two-photon excitation cross sections of molecular fluorophores with data from 690 to 1050 nm," J. Opt. Soc. Am. B **13,** 481–491 (1996).
10. J. Fishkin, O. Coquoz, E. Anderson, M. Brenner, and B. Tromberg, "Frequency-domain photon migration measurements of normal and malignant tissue optical properties in a human subject," Appl. Opt. **36,** 10–20 (1997).
11. C. Sheppard and M. Gu, "Image formation in two-photon fluorescence microscopy," Optik **86,** 104–106 (1990).
12. S. Jacques, C. Alter, and S. Prahl, "Angular dependence of HeNe laser light scattering by human dermis," Lasers Life Sci. **1,** 309–333 (1987).
13. A. Dunn and R. Richards-Kortum, "Three-dimensional computation of light scattering from cells," IEEE J. Sel. Top. Quantum Electron. **2,** 898–905 (1997).
14. H. van Staveren, C. Moes, J. van Marle, S. Prahl, and M. van Gemert, "Light scattering in Intralipid-10% in the wavelength range of 400–1100 nm," Appl. Opt. **30,** 4507–4514 (1991).
15. C. L. Smithpeter, A. K. Dunn, A. J. Welch, and R. Richards-Kortum, "Penetration depth limits of *in vivo* confocal reflectance imaging," Appl. Opt. **37,** 2749–2754 (1998).
16. V. Centonze and J. White, "Multiphoton excitation provides optical sections from deeper within scattering specimens than confocal imaging," Biophys. J. **75,** 2015–2024 (1998).
17. H. Kume, ed., Hamamatsu Photonics, *Photomultiplier Tube: Principle to Application*," (Hamamatsu Photonics, Bridgewater, N.J., 1994).
18. R. Hornung, T. Pham, K. Keefe, J. Fishkin, M. Berns, Y. Tadir, and B. Tromberg, "Quantitative near infrared spectroscopy of cervical dysplasia *in vivo*," Hum. Reprod. **14,** 2908–2916 (1999).
19. T. Farrel, B. Wilson, M. Patterson, and M. Olivio, "Comparison of the in vivo photodynamic threshold dose for photofrin, mono- and tetrasulfonated aluminum phthalocyanine using a rat liver model," Photochem. Photobiol. **68,** 394–399 (1998).
20. D. Oh, R. Stanley, M. Lin, W. Hoeffler, S. Boxer, M. Berns, and E. Bauer, "Two-photon excitation of 4′-Hydroxylmethyl-4,5′,8-Trimethylpsoralen," Photochem. Photobiol. **65,** 91–95 (1997).

128.200.102.124 {ts '2016-11-08 11:45:55'}